Received: 24 July 2023 | Revised: 29 October 2023 | Accepted: 9 November 2023

DOI: 10.1002/pamm.202300300

RESEARCH ARTICLE

Latent heat effects in inductive heating of shape memory alloy fibers

Stefan Descher[1] | **Philipp Krooß**[2] | **Felix Ewald**[2] | **Sebastian Wolf**[1] | **Detlef Kuhl**[1]

[1]Institute of Structural Mechanics, University of Kassel, Kassel, Germany

[2]Institute of Materials Engineering, Metallic Materials, University of Kassel, Kassel, Germany

Correspondence
Stefan Descher, Institute of Structural Mechanics, University of Kassel, Mönchebergstr. 7, 34125 Kassel, Germany.
Email: descher@uni-kassel.de

Abstract

Motivation of the present work is an inductive heating process, used in manufacturing a new kind of improved ultra-high performance concrete. In this novel material, fibers made out of shape memory alloys are used to increase the maximum possible fiber volume fraction, or to create an internal state of compressive stress. In contrast to other works, the underlying microstructure transformation from martensite to austenite is highlighted based on thermal analysis. Dynamic scanning calorimetry measurements are adapted as basis for development of a phenomenological phase transformation model. It relates local temperature and temperature rate to the rate of change of the phase indicator, modeling the transformation of martensite to austenite. Latent heat is considered by an enthalpy method, the inductive heating process is considered by a phenomenological model. Study results for a purely thermodynamic process of heating a single fiber embedded in concrete are presented. They show that latent heat effects delay phase transformation and the process of fiber activation is very sensitive to the induced heat. Furthermore, it is discovered that latent heat causes a strongly inhomogeneous state of transformation in radial direction of the fiber, which is of great importance for thermomechanical processes and the interpretation of experimental results.

1 | INTRODUCTION

Reinforcing ultra-high performance concrete (UHPC) using steel fibers is a common proceeding in civil engineering. Most importantly, thereby, brittle behavior of plain UHPC is transformed to ductile, which increases its applicability vastly. This improved material stands out because it enables manufacturing relatively slender and much more durable structures. Further improvement is obtained by using fibers made out of iron-based [1] shape memory alloys (SMAs), as recent works propose [2, 3]. They enable to obtain a higher fiber volume fraction by influencing the rheology of fresh concrete [4] or to create a state of internal compression [5]. The first goal can be achieved by using rolled up fibers in the casting process, which reduces fiber-fiber interaction. This leads to less clumping and allows to increase the maximum possible fiber fraction. Afterwards, the fibers are straightened by activating the one-way effect due to heating them up. The second goal can be achieved by using pre-stretched fibers. After curing of the concrete matrix, their one-way effect can be activated

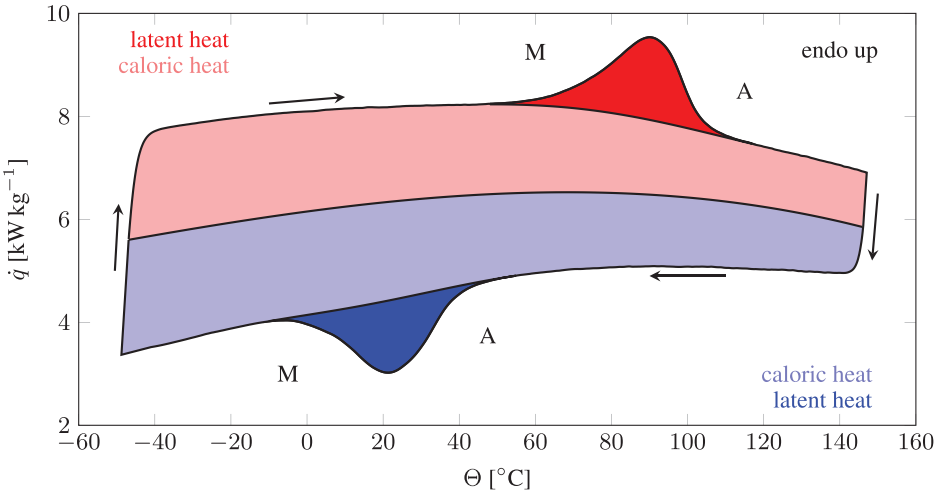

FIGURE 1 DSC scan for NiTiHf, recorded for the temperature range from -50 °C to 150 °C at $\dot{\Theta}_{DSC} = 20\,°C\,min^{-1}$ with a sample mass of 11.94 mg under Nitrogen atmosphere. In "endo up" representation, endothermic processes cause positive peaks. The experiment's thermal direction is annotated with arrows. Areas corresponding to caloric heat are drawn lighter than those, that are considered as latent heat. The two bell curves are caused by the phase transformation from martensite (M) to austenite (A) and vice versa.

thermally as well, which leads to tension in the fibers and compression in the surrounding concrete. In both cases, inductive heating is proposed, since conduction-based methodologies would require heating up large volumes of material. Works focusing on numerical modeling and simulation of induction heating are ref. [6, 7]. The present work approaches this process from the standpoint of the material's thermodynamic behavior and its role in this process using an additively manufactured NiTi based SMA as a model alloy in order to simulate the phase transformation, since the characteristic transformation temperatures associated with the martensitic phase transformation are well understood in these alloys. In this case, the material was processed by Laser Powder Bed Fusion (L-PBF). Details on the manufacturing process can be found in ref. [8].

The present work is motivated by two well-known principles, that are united in the inductive heating process. Firstly, that the effectiveness of induction coils drops strongly in distance, see ref.[9]. Secondly, that the activation of the one-way effect in SMAs is an endothermic process [10]. This means, a heating system of which the effective heating power strongly depends on operation conditions should be used to drive a physical process that can only be completed if it is fed sufficiently. Consequently, it is of great importance to understand the role of the energy that is consumed during phase transformation in this inductive heating processes.

2 | THERMAL ANALYSIS BASED ON DIFFERENTIAL SCANNING CALORIMETRY

The mechanical behavior of SMAs is commonly displayed in stress-strain-temperature curves, see for example ref. [11]. They reveal, that for SMAs, a pseudo-plastic strain can be brought into the material, which can be retrieved by heating. It is the one-way effect, that straightens the fibers or creates an internal state of compression. It is enabled by a change in microstructure, that is a phase transformation from martensite to austenite. To gather such information, normally a certain tensile test program is executed in a furnace. A totally different approach is performing investigations in a Differential Scanning Calorimetry (DSC, [12]) under the absence of mechanical load. A DSC allows to detect any heat flux emitted or adsorbed by a sample in isothermal or non-isothermal conditions. Therefore, it is possible to quantify the heat flow that is connected to the phase transformation. Since a heating process is object of study, the experiment is performed in non-isothermal conditions. This means a certain temperature range is chosen, which is investigated with a certain heating/cooling rate resp. temperature rate $\dot{\Theta}_{DSC}$. As a result, the specific heat flux $\dot{q}$ over temperature Θ, is evaluated. In Figure 1, it is displayed for a high temperature Nickel-Titatium-Hafnium (NiTiHf) alloy, which is used as a benchmark in the present work, due to its well-known endothermic and exothermic heat flux associated with the phase transformation. Regarding the temperature level for activation, it is similar to the iron-based alloys that are intended to be used in the new kind of UHPC.

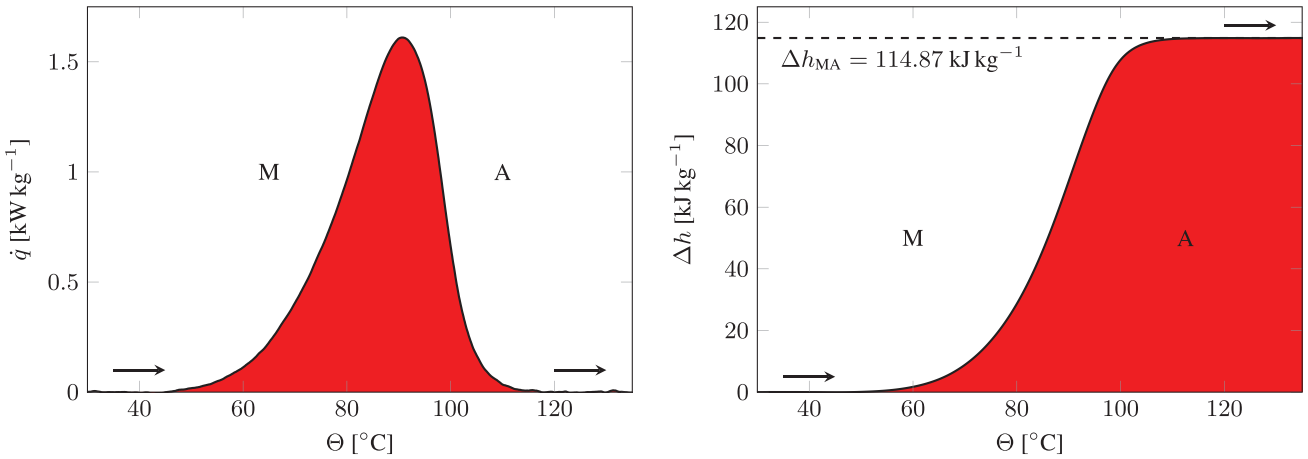

FIGURE 2 Evaluation of the M→A peak of Figure 1. The left plot was generated by subtracting the caloric part of the signal based on a polynomial of degree seven. The right plot shows the integrals function of the left plot, that is divided by the heating rate, see Equation (1). Its final value corresponds to the enthalpy change during phase transformation.

It shows that the overall signal forms a hysteresis and can be divided into four regions. The two caloric regions that divide the center region equally, and two bell-shaped latent heat regions that are caused by the M→A and A→M phase transformation. Note that the M→A phase transformation, which is core of the present work, is an endothermic process. It means that in the heating process, additional heat has to be provided. The lower part of the hysteresis reveals that in a cooling process, additional heat has to be removed. Furthermore, there is a pronounced temperature difference between the two phase transformation regions. It is useful for modeling, since this means, if during the M→A phase transformation, temperature only decreases slightly, austenite will not transform back to martensite. Since the temperature gap separating the two peak tips is approximately 70°C, the model of the present work will be defined as one directional.

To transform the results in a usable form for modeling the M→A phase transformation, a separation of the upper latent heat peak from the overall signal is needed, see ref. [13]. This was executed by modeling the caloric heat signal in the range from −40°C to 140°C using a polynomial of degree seven. It was already used for separating the caloric and latent heat regions in Figure 1. The result is the bell curve of Figure 2 left, of which the integral

$$\Delta h(\Theta) = \frac{1}{\dot{\Theta}_{\mathrm{DSC}}} \int \dot{q}(\Theta) \mathrm{d}\Theta \tag{1}$$

corresponds to the enthalpy absorbed by the transformation. When the M→A phase transformation is finished, $\Delta h(\Theta)$ reaches a limit value Δh_{MA}, which will later be used as the transformation enthalpy Δh_{tr}. Its meaning is the same as for example a melting enthalpy, therefore a modeling approach from this field of research is applied.

3 | MODELING AND SIMULATION OF THE PHASE TRANSFORMATION

Gaining information about the progress of phase transformation is possible by dividing the curve presented in Figure 2 right by its maximum. The result is the phase indicator function $\phi(\Theta)$, which for $\phi = 0$ corresponds to martensite and for $\phi = 1$ to austenite, see Figure 3 . The present work intends to model this progress phenomenologically and derive an evolution equation by differentiation, as done in ref. [14]. For this purpose, the normalized error function

$$\phi(\Theta) = \frac{1}{2}\left[1 - \mathrm{erf}\left(\frac{4\sqrt{\ln 2}(\Theta_{\mathrm{tr}} - \Theta)}{\Delta\Theta_{\mathrm{tr}}}\right)\right] \tag{2}$$

is chosen. It is based on the transformation temperature $\Theta_{\mathrm{tr}} = \Theta(\phi = 0.5)$ and the transformation temperature range $\Delta\Theta_{\mathrm{tr}}$, which corresponds to the temperature range, the transformation takes place. For the given NiTiHf, the latter was determined as $\Delta\Theta_{\mathrm{tr}} = 47.75$°C using least squares, $\Theta_{\mathrm{tr}} = 87.5$°C was read directly from the data.

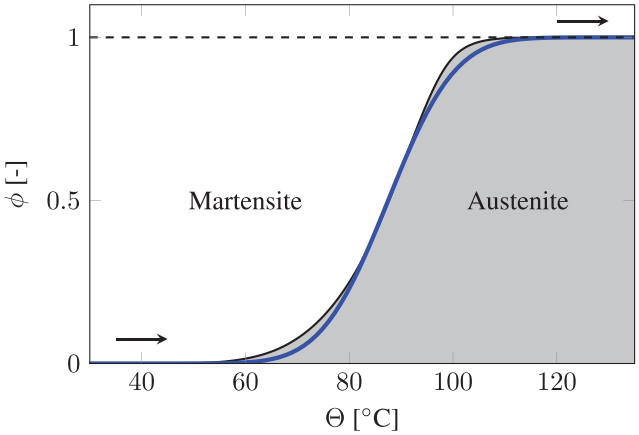

FIGURE 3 Experimentally derived phase indicator compared to the empirical function given by Equation (2), plotted in blue. Martensite corresponds to $\phi = 0$, austenite to $\phi = 1$.

The evolution equation for ϕ is obtained by calculating the total differential. However, it is limited to positive values to ensure that ϕ cannot decrease. This property was discussed regarding Figure 1 based on the temperature difference between the two regions of phase transformation. Consequently,

$$\dot{\phi}(\Theta, \dot{\Theta}) = \max\left(0, \frac{\mathrm{d}\phi}{\mathrm{d}\Theta}\frac{\partial\Theta}{\partial t}\right) \tag{3}$$

has to be solved for the initial condition $\phi(t = 0) = 0$. It is possible to calculate the first expression of the differential analytically. Therefore, during the simulation,

$$\frac{\mathrm{d}\phi}{\mathrm{d}\Theta} = \sqrt{\frac{4\ln 2}{\pi\Delta\Theta_{\mathrm{tr}}}}\exp\left(-4\ln 2\frac{(\Theta_{\mathrm{tr}} - \Theta)^2}{\Delta\Theta_{\mathrm{tr}}^2}\right) \tag{4}$$

has to be adapted to local temperature. The temperature rate $\dot{\Theta}$ is obtained by the numerical solution of the energy balance.

A heat sink is used to consider the absorption of heat, denoted as Q_{tr}. Its magnitude is proportional to the rate of change of ϕ, following the standard enthalpy method [15], known from phase field methods [16]. The resulting energy equation is

$$\rho c\,\dot{\Theta} + \nabla\cdot(-\lambda\nabla\Theta) = Q_{\mathrm{tr}} + Q_{\mathrm{J}}, \qquad Q_{\mathrm{tr}} = -\rho\Delta h_{\mathrm{tr}}\frac{\partial\phi}{\partial t}. \tag{5}$$

For this consideration to work as desired, meaning that the absolute heat absorbed is limited to the latent heat, a second limiter ensuring that $\phi \leq 1$ has to be introduced, for example demonstrated in ref. [13]. It deactivates the source term of Equation (3) for $\phi \geq 1$. Next to density ρ, heat capacity c and heat conductivity λ, a term considering inductive heating appears, denoted as JOULE heat source Q_{J}. If a simulation of MAXWELL's equations is desired, it is proportional to the local electric field. However, in the present work, a phenomenological approach is chosen. It is to set Q_{J} different from zero only in regions close to the fiber's surface, further described in the following chapter.

Equation (2) and Equation (4) are solved using an in house finite element solver. For spatial discretization biquadratic LAGRANGE elements are used, temporal discretization is carried out by application of the NEWMARK-α-method with a parameter setting for implicit treatment. The energy and phase indicator equations are coupled on the GAUSS quadrature point weakly, Θ is updated first in every time step.

4 | FIBER ACTIVATION STUDIES

Studies are performed for the inductive heating process of a single SMA fiber embedded in concrete, described in Figure 4. It is an axisymmetric setup in which the materials are assigned on an element level. Standard coefficients for steel and concrete are used in the energy equation. Only in the outer element layer of the fiber, the inductive heat source is different

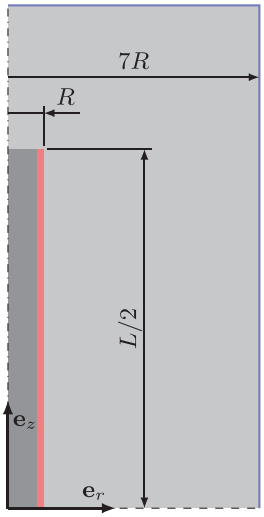

Domains

- SMA w/o heat source
- SMA w/ heat source
- concrete

Boundaries

- $\Theta = 20\,^{\circ}\mathrm{C}$
- axial symmetry
- planar symmetry

Dimensions

- $R = 0.5$ mm
- $L = 10$ mm

Material Properties

Domain	ρ [kg m^{-3}]	c [J (kg K)$^{-1}$]	λ [W (m K)$^{-1}$]	Δh_{tr} [J kg^{-1}]	Q_{J} [W m^{-3}]
SMA w/o Q_{J}	7850	500	50	114.87e+3	0
SMA w/ Q_{J}	7850	500	50	114.87e+3	1e+10
concrete	2500	1000	2	0	0

FIGURE 4 Domains, boundary conditions, dimension and material properties for the single SMA fiber embedded in concrete. The red domain's thickness is one finite element, the overall resolution is 10 biquadratic LAGRANGE-elements over the fiber radius.

from zero. In this way, it is considered that inductive heating systems are generally most dominant in surface-close regions, see for example ref. [6, 17, 18]. This approach was already used in ref. [5] and is suited very well for parameter studies. Alternatively, the MAXWELL equations could be solved numerically for the fiber, coil and environment [6, 18]. However, since the effort of solving the coupled electromagnetic and thermal field is very high, the present phenomenological inductive heat model is used.

The initial condition is the static state at 20°C, which is also the outer boundary temperature. The fiber length is 10 mm and its diameter is 1 mm, the outer dimension of the compound is 15 mm by 7 mm. At $z = 0$, a planar symmetry boundary condition is applied. A resolution of 20 elements/mm and a time step size of 0.5 ms was found out to be sufficient for the presented studies. Note that in this process, the criterion for time step size is Equation (3), since otherwise $\phi = 1$ will not be reached or the value will be exceeded vastly. Furthermore, the value of $Q_{\mathrm{J}} = 1\mathrm{e}{+10}$ W m^{-3} in the outer fiber element layer is indeed quite large. However, it ensures fast heating which triggers the phase transformation almost immediately. Furthermore, if for such a high value of Q_{J} there is an influence of latent heat, there will certainly be one for lower values.

In order to study the influence of latent heat, a parameter study was performed for the parameter $\Delta h_{\mathrm{tr}} = \Delta h_{\mathrm{MA}}$, of which the results are displayed in the two left plots of Figure 5. It shows that when neglecting latent heat, standard exponential heating occurs. When taking latent heat into account, this process is delayed by formation of an almost isothermal range that extends with increased latent heat. It is not exactly isothermal, because the temperature rate drives the phase transition, see Equation (3). This indicates that a large amount of the induced heat is absorbed by the phase transformation. Therefore, the heat sink reached a magnitude, at which this condition is enabled. Since the magnitude of the heat sink is proportional to the rate of change of ϕ, this means for lower values of Δh_{tr}, higher transformation rates occur and vice versa. It is exactly the outcome of the presented parameter study. Since the parameter setup for 100% Δh_{MA} is already realistic, it can be concluded that for SMA fibers as they are supposed to be used for creating a new kind of UHPC, latent heat plays an important role in the inductive heating process.

The motivation to study the influence of Q_{J} is in its great dependence on the operating conditions of the induction coil. One obvious influence is, that for smaller Q_{J}, the time constant of exponential heating is larger. As a result, it takes longer until the transformation is triggered. That the transformation takes place at the same temperature level for all values of Q_{J} investigated, shows that it is caused by the transformation. Since at the same fiber temperature, the heat flux towards the cooled boundaries must be in the same range, because it is temperature gradient-related, different amounts of heat are available to drive the phase transformation. This means, for lower values of Q_{J}, the phase transformation takes longer. It is assumed, that if Q_{J} is barely sufficient to heat up the fiber into the temperature range of transformation, it is not realistic that the whole SMA domain transforms into austenite in a technical process. This is exclusively caused by latent heat and has to be considered in design of such a process and thermomechanical models.

Besides the influence of latent heat on temporal changes of ϕ, it is also important to know about its influence on spatial distribution. The reason is that due to the phase transformation, strain is released, which is extensively discussed in the preceding work of this paper [5]. Consequently, the distribution of ϕ can be related to the stress distribution. This is,

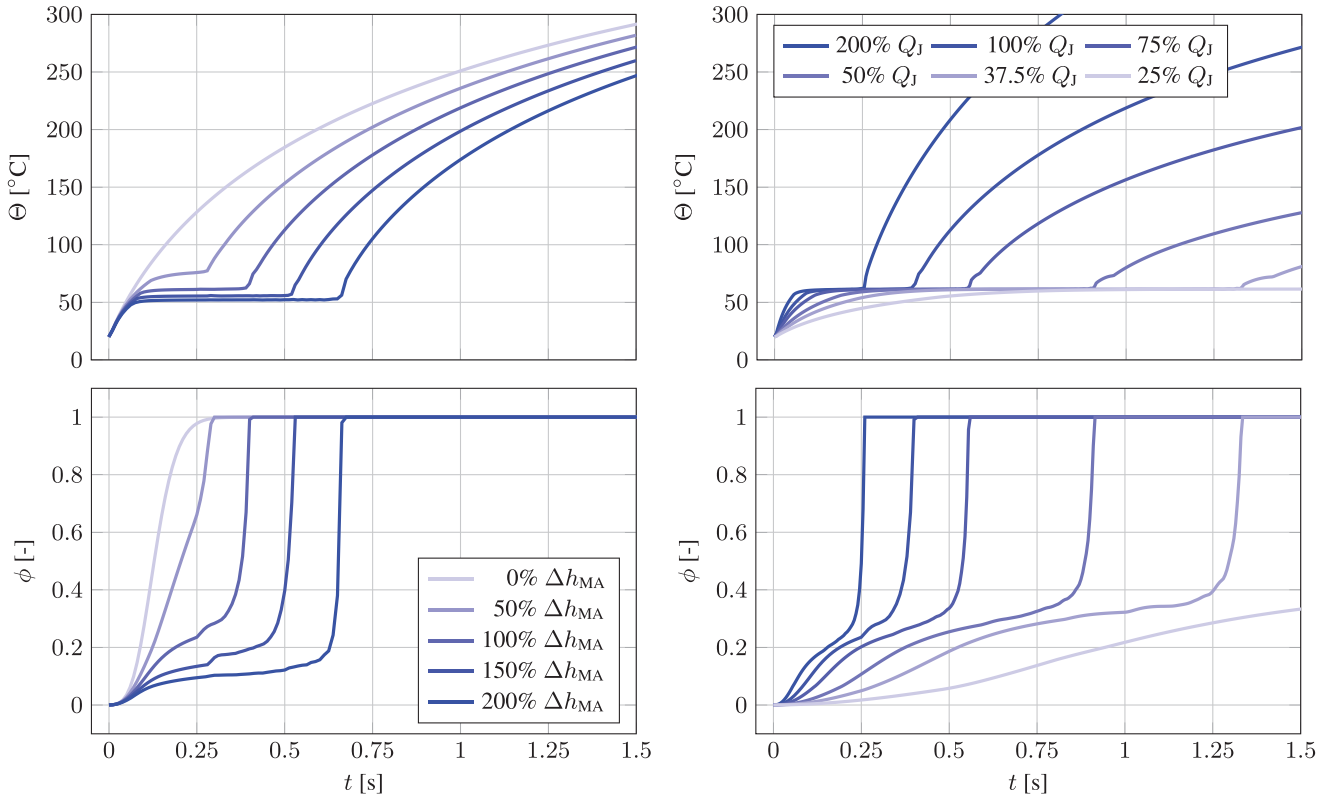

FIGURE 5 Parameter studies performed for the impact latent heat and JOULE heating. In both left plots, Δh_{tr} is varied while Q_J is constant. In both right plots, Q_J is varied while Δh_{tr} is constant. Temporal progress of the phase indicator and temperature are plotted for the coordinate $(r = 0, z = 0)$.

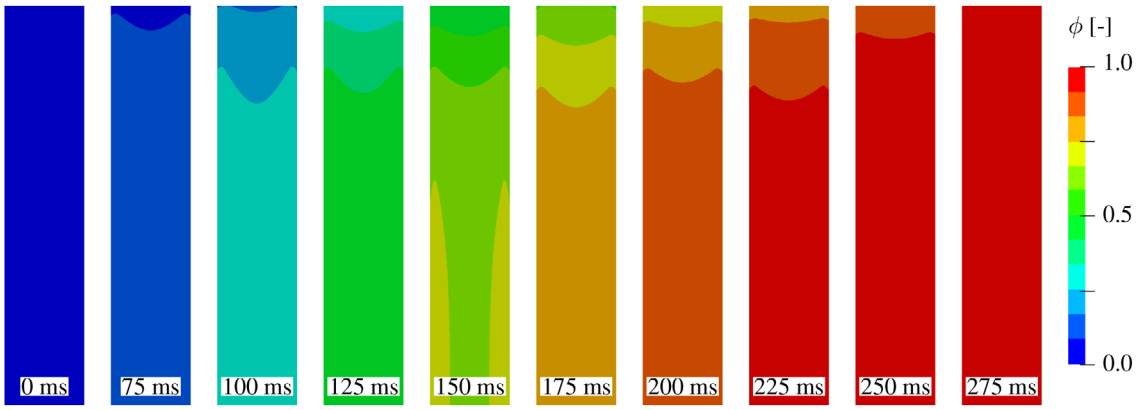

FIGURE 6 Progress of the phase indicator during fiber activation for $\Delta h_{tr} = 0$. Only the upper half of the fiber is displayed.

for example, vital for the process of unfolding SMA fibers in fresh concrete. When analyzing the phase indicator field during transformation, one key influence of latent heat stands out. If latent heat is neglected, shown in Figure 6, the transformation occurs smoothly over the radius. There is only a small positive gradient towards the outer region, because this is where $Q_J \neq 0$. However, its magnitude is much smaller than the magnitude of the negative gradient towards the tips.

If latent heat is considered, the result is totally different, as shown in Figure 7. A transformation zone is forming and moves from the outer region of the fiber, towards the center. This is in superposition with the previously observed gradient towards the tip. As a result, a cusp-shaped isoline of $\phi = 1$ moves from $(r = 0, z = 0)$ towards $(r = 0, z = L/2)$ until the fiber is fully austenitic.

Considering, that in parts with multiple fibers included, the distribution of induced heat is highly irregular and certainly not axisymmetric on a fiber level, this finding is crucial. It means that in the fiber's thickness direction, there are

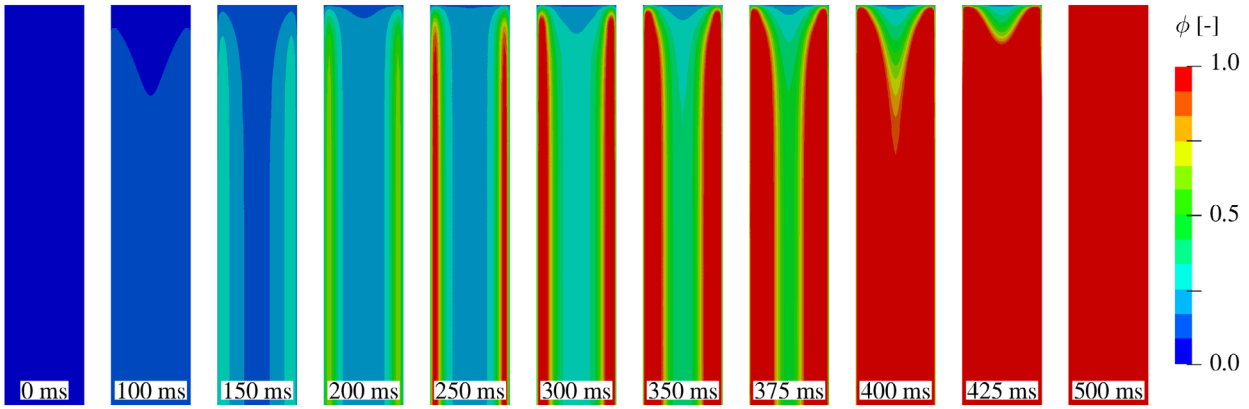

FIGURE 7 Progress of the phase indicator during fiber activation for $\Delta h_{\mathrm{tr}} = \Delta h_{\mathrm{MA}}$. Only the upper half of the fiber is displayed.

for example interactions between transformed and untransformed zones. When realizing the above-described process of unrolling fibers on the basis of a beam model, this influence must be considered in addition to the lengthwise gradient of phase transformation.

The existence of such a transformation zone is typical for systems with sufficient influence of latent heat. It is often found in fluid to solid transformations such as melting and there are many works focusing on it, a popular is ref. [19]. Consequently, this finding is plausible. That the phase transformation will always start at a surface is justified by the principle of working of inductive heatings. As they can only act in the surface regions of metallic objects, this is where temperatures increase first.

5 | CONCLUSIONS AND OUTLOOK

Major conclusion of the present work is that it is absolutely necessary to consider latent heat effects in induction heating cases that involve SMAs. Because of the strong decrease in effectiveness of the JOULE heating impact, a sufficient heat source driving the martensite to austenite transformation might not be reached. The result might be an incomplete respectively stuck activation. It is important to consider, that latent heat effects might extend activation time vastly. When considering to describe the activation mechanically, based on a beam model, it must be considered that latent heat causes a strongly inhomogeneous state of transformation, that will affect stresses greatly.

The continuation of the present work is to consider coupling of the phase transformation and temperature to the momentum equation, as done in the preceding work [5]. It allows to investigate the influence of latent heat in tensile tests, as they are usually performed to generate the well-known stress-strain-temperature curves.

ACKNOWLEDGMENTS

Open access funding enabled and organized by Projekt DEAL.

ORCID

Stefan Descher https://orcid.org/0000-0001-9031-7340

REFERENCES

1. Niendorf, T., Brenne, F., Krooß, P., Vollmer, M., Günther, J., Schwarze, D., & Biermann, H. (2016). Microstructural evolution and functional properties of Fe-Mn-Al-Ni shape memory alloy processed by selective laser melting. *Metallurgical and Materials Transactions A*, *47*, 2569–2573.
2. Schleiting, M., Wetzel, A., Gerland, F., Niendorf, T., Wünsch, O., & Middendorf, B. (2020). Improvement of UHPFRC-rheology by using circular shape memory alloy fibres. *Rheology and Processing of Construction Materials*, *23*, 142–148.
3. Vollmer, M., Bauer, A., Frenck, J.-M., Krooß, P., Wetzel, A., Middendorf, B., Fehling, E., & Niendorf, T. (2021). Novel prestressing applications in civil engineering structures enabled by Fe–Mn–Al–Ni shape memory alloys. *Engineering Structures*, *241*, 112430.
4. Gerland, F., Schomberg, T., Kuhl, D., & Wünsch, O. (2021). Flow and fiber orientation of fresh fiber reinforced concrete. *Proceedings in Applied Mathematics and Mechanics*, *21*, 202100109.

5. Descher, S., Krooß, P., Kuhl, D., Wetzel, A., & Wolf, S. (2023). Internal prestressing of ultra-high performance concrete using shape memory fibers. *Proceedings in Applied Mathematics and Mechanics*, *23*, e202200253.
6. Gleim, T. (2016). *Simulation of manufacturing sequences of functionally graded structures*. Kassel University Press.
7. Gleim, T., Kuhl, D., Schleitling, M., Wetzel, A., & Middendorf, B. (2019). High-order numerical methods for the thermal activation of SMA fibers. *Proceedings in Applied Mathematics and Mechanics*, *19*, e201900025.
8. Sajadifar, S. V., Krooß, P., Ewald, F., Lauhoff, C., Bolender, A., Kahlert, M., Gerstein, G., & Niendorf, T., in preparation (2023).
9. Rudnev, V., Loveless, D., Cook, R., & Black, M. (2003). *Handbook of Induction Heating*. Marcel Dekker.
10. Boyd, J. G., & Lagoudas, D. C. (1996). A thermodynamical constitutive model for shape memory materials. Part I. The monolithic shape memory alloy. *International Journal of Plasticity*, *12*, 805–842.
11. Hartl, D. J., & Lagoudas, D. C. (2007). Aerospace applications of shape memory alloys. *Proceedings of the Institution of Mechanical Engineers, Part G: Journal of Aerospace Engineering*, *221*, 535–552.
12. Höhne, G. W. H., Hemminger, W., & Flammersheim, H.-J. (1996). *Differential scanning Calorimerty*. Springer, Heidelberg.
13. Descher, S. (2020). *Modeling and simulation of crystallization processes in polymer melt flows*. Kassel University Press.
14. Descher, S., & Wünsch, O. (2022). Simulation framework for crystallization in melt flows of semi-crystalline polymers based on phenomenological models. *Archive of Applied Mechanics*, *92*, 1859–1878.
15. Voller, V. R., Cross, M., & Markatos, N. C. (1987). An enthalpy method for convection/diffusion phase change. *International Journal for Numerical Methods in Engineering*, *24*, 271–284.
16. Beckermann, C., Diepers, H.-J., Steinbach, I., Karma, A., & Tong, X. (1999). Modeling melt convection in phase-field simulations of solidification. *Journal of Computational Physics*, *154*, 468–496.
17. Gleim, T., Schröder, B., & Kuhl, D. (2015). Nonlinear thermo-electromagnetic analysis of inductive heating processes. *Archive of Applied Mechanics*, *85*, 1055–1073.
18. Gleim, T., & Kuhl, D. (2019). Electromagnetic analysis using high-order numerical schemes in space and time. *Archives of Computational Methods in Engineering*, *26*, 405–447.
19. Costa, M., Buddhi, D., & Oliva, A. (1998). Numerical simulation of a latent heat thermal energy storage system with enhanced heat conduction. *Energy Conversion and Management*, *39*, 319–330.

How to cite this article: Descher, S., Krooß, P., Ewald, F., Wolf, S., & Kuhl, D. (2023). Latent heat effects in inductive heating of shape memory alloy fibers. *Proceedings in Applied Mathematics and Mechanics*, *23,* e2300300. https://doi.org/10.1002/pamm.202300300